Heliyon 10 (2024) e39951

Contents lists available at ScienceDirect

Heliyon

journal homepage: www.cell.com/heliyon

Research article

Upconversion luminescence and thermosensitive properties of $NaGd(PO_3)_4:Yb^{3+}/Er^{3+}$

Jintao Xu [a], Shanlin Zhu [a], Canyuan Liao [a], Weijun Zhao [a], Xingyuan Zhong [a], Zijun Wang [b,**], Jiuping Zhong [a,*]

[a] School of Materials, Sun Yat-Sen University, Shenzhen, 518107, China
[b] L'Institut Mondor de Recherche Biomédicale, Université Paris Est Créteil, INSERM, U955, CNRS, 94010, Créteil, France

ARTICLE INFO

Keywords:
Phosphates
Upconversion
Fluorescence intensity ratio
Thermal sensing

ABSTRACT

High-sensitivity optical temperature measurement has attracted extensive attention in both fundamental studies and practical applications. In this study, a series of upconversion (UC) luminescence phosphors composed of $NaGd(PO_3)_4$ (NGP) doped with 20 at% Yb^{3+} and various concentrations of Er^{3+} (0.5 at% as the optimal concentration) was synthesized by high-temperature solid-state method. And their crystal structure and the distribution of lanthanide dopants were analyzed using X-ray diffraction with Rietveld refinement verifies. Under 980 nm laser excitation, the obtained phosphors show the characteristic Er^{3+} upconversion green and red emission bands through two-photon processes. The fluorescence intensity ratio (FIR) based on the thermal coupled states demonstrates the thermal sensing ability in a wide temperature range of 200–573 K. The thermal sensitivity is relatively high with the maximum absolute thermal sensitivity S_a of 0.53 % K^{-1} (523 K) and the maximum relative thermal sensitivity S_r of 2.60 % K^{-1}. The phosphor NGP:Yb/Er also exhibits high repeatability as the thermal sensors reach 97 %. These findings postulate the potential of NGP:Yb/Er as a promising candidate in optical thermal sensing applications.

1. Introduction

Lanthanide (Ln^{3+})-doped upconversion (UC) luminescence materials have attracted significant attention due to their exceptional optical properties and diverse applications in the fields of optical thermometry [1], anti-counterfeiting [2], bioimaging and therapy [3], and super-resolution imaging [4]. Ln^{3+}-doped UC phosphors exhibit distinct advantages over traditional temperature sensing techniques, including non-invasive measurement, short response time and high sensitivity. Among the various contactless approaches, fluorescence intensity ratio (FIR)-based optical temperature sensing has emerged as a leading technique, owing to its resistance to external fluctuations (e.g. excitation power and thus fluorescence intensity) and its ability to achieve high-precision and wide-range temperature measurements [5].

The principle of FIR temperature sensing relies on the thermal coupling of adjacent energy levels in lanthanides, typically with energy differences (ΔE) in the range of 200–2000 cm^{-1}. Under excitation, these energy levels rapidly reach a "thermal equilibrium" state, in which the electron population follows Boltzmann's law [6]. Lanthanides possessing suitable thermal coupled energy levels

* Corresponding author.
** Corresponding author.
E-mail addresses: zijun.wang@inserm.fr (Z. Wang), zhongjp@mail.sysu.edu.cn (J. Zhong).

https://doi.org/10.1016/j.heliyon.2024.e39951
Received 2 September 2024; Received in revised form 27 October 2024; Accepted 28 October 2024
Available online 29 October 2024

such as Er^{3+}, Pr^{3+}, Eu^{3+}, Nd^{3+} and Ho^{3+}, have been extensively used for optical temperature measurement [7]. For the Yb-Er system, Yb^{3+} as a sensitizer provides a large absorption cross section (~ 11. 7 × 10^{-21} cm^2) for the near-infrared radiation (976 nm) and Er^{3+} ion acts as an activator due to its intra f-f transitions [8].

UC emission is a result of multi-step photon processes. The UC efficiency is influenced by multi-phonon relaxation rates significantly, which in principle should be low to minimize non-radiative energy loss. Fluoride and chloride are examples but often suffer from poor stability and pose environmental risks. Despite their relatively high phonon energies, oxide-based materials have been often considered promising hosts for UC applications due to their excellent chemical and physical stability [9]. Notably, certain oxide materials, such as $SrWO_4$, $CaMoO_4$ and $YNbO_4$, have been demonstrated exceptional thermal sensitivity based on thermally coupled energy levels of Er^{3+} ions [10–12]. Researchers also have attempted to improve the optical properties and temperature measurement performance of Er^{3+}/Yb^{3+} co-doped oxides by adding Li^{+}, Bi^{3+} ions, core-shell coating methods, etc [13–15]. However, the high sensitivity and wide range of host materials are still the direction pursued by researchers [16].

In previous studies, $MGd(PO_3)_4$ (M = Li, Na, K, Cs) has been identified as excellent host materials with non-deliquescent nature, low-temperature synthesis, and superior physical and chemical properties. Furthermore, Gd^{3+} ions act as intermedia to facilitate efficient energy transfer to emitter ions, such as Ce^{3+}, Eu^{3+}, Tb^{3+} and Dy^{3+} [17]. In this study, Yb^{3+}/Er^{3+} co-doped $NaGd(PO_3)_4$ (NGP) phosphors were synthesized by the solid-state method, and the structure and UC properties were investigated comprehensively. This work aims to explore the luminescence performance, energy transfer mechanisms and temperature sensing capabilities of NGP:Yb/Er, so as to develop advanced optical thermometry materials.

2. Experiments

2.1. Preparation

The phosphors were synthesized through a high-temperature solid-state reaction method according to the chemical reaction of eq. (1). Stoichiometric amounts of $NH_4H_2PO_4$ (AR, Hushi), Gd_2O_3 (99.99 %), Er_2O_3 (99.99 %), Yb_2O_3 (99.99 %), Na_2CO_3 (GR, >99.8 %), C_2H_5OH (AR, Guangdong Sci-Tech) were thoroughly mixed and heated up to 973 K gradually, which was maintained for over 12 h. All chemical reagents were sourced from Aladdin unless otherwise specified, and all raw materials were used as received without further processing.

$$8NH_4H_2PO_4 + (0.8-x)Gd_2O_3 + xEr_2O_3 + 0.2Yb_2O_3 + Na_2CO_3 \xrightarrow[12h]{973K} 2NaGd_{0.8-x}Er_xYb_{0.2}(PO_3)_4 + 12H_2O + 8NH_3\uparrow + CO_2\uparrow \quad (1)$$

2.2. Characterization

The crystal structure of synthesized phosphors was characterized by X-ray diffraction (XRD, BRUKER D8 ADVANCE, 40 kV, 40 mA). Raman spectroscopy was examined using a Raman spectrometer (InVia Qontor) under 488 nm laser excitation (Modu Laser). Scanning electron microscopy (SEM) was performed on a Hitachi SU5000 microscope (15 kV) coupled with energy dispersive spectroscopy (EDS). Steady-state spectra were recorded on a fluorescence spectrometer (Edinburgh FLS1000) with a photomultiplier detector (RP928, 300–980 nm), a continuous wave 980 nm laser diode as an excitation source (MDL-III-980-2W) and heaters (MicrostatN, 77–300 K; Tianjin Dongfang Kejie Technology Co., Ltd, 298–573 K). Lifetime spectra were also collected with the 980 nm laser diode in pulse mode (pulse width = 2 ms). UV–Vis diffuse reflectance spectroscopy was measured using a UV–Vis–NIR spectrophotometer (Shimadzu UV-3600).

2.3. Theoretical calculation

Density functional theory (DFT) calculation was performed using the Vienna Ab initio Simulation Package (VASP) [18]. The Perdew-Burke-Ernzerhof (PBE) function within the generalized gradient approximation (GGA) was employed to describe electron exchange-correlation potentials [19]. The kinetic energy cutoff was set to be 400 eV for the plane-wave basis set. Structure optimization was carried out with a maximum force of 0.01 eV $Å^{-1}$ and self-consistent calculations were converged to an energy threshold of 1 × 10^{-5} eV. Brillouin zone integrals were sampled using 2 × 2 × 3 Monkhorst−Pack grid k-points for NGP and the grid k-points were generated by the Monkhorst−Pack scheme for density of states.

Band structure and band gap (E_g) values were computed using the DFT + U approach, incorporating the rotationally invariant approach to GGA + U proposed by Dudarev et al. [20]. Correlations were included within the DFT + U scheme for the localized f manifold of Gd^{3+}, with a Hubbard U term being 6.0 eV obtained from the Materials Project [21].

3. Results and discussion

3.1. Crystal structure and morphology

A series of NGP:20YbxEr phosphors were synthesized doping with 20 at% Yb^{3+} and various concentrations of Er^{3+} (x = 0.3, 0.5, 1,

1.5, 2 at%). Their XRD patterns aligned with the standard card (PDF#47–0657) are shown in Fig. 1a. It can be found that the doping of Er^{3+} and Yb^{3+} does not alter the crystal structure of NGP. The NGP phosphors crystallize in a monoclinic phase with a $P2_1$ space group. Because the ionic radius of doping Er^{3+} (0.089 Å) and Yb^{3+}(0.868 Å) are close to the radii of Gd^{3+} (0.938 Å) in the host NGP, Er^{3+} and Yb^{3+} ions are expected to fully substitute Gd^{3+} sites although the spatial structure of $P2_1$ is not conducive to high Yb^{3+} concentration (Fig. S1) [22]. The observed shift of XRD diffraction peaks towards higher angles when Er^{3+} and Yb^{3+} ions with smaller ionic radii replace Gd^{3+} ions at larger positions, which indicates the Gd^{3+} sites in the host NGP were substituted successfully by Er^{3+} and Yb^{3+} ions. Rietveld refinement (Fig. 1b) of the NGP host using GSAS yielded refinement indicators of $R_{wp} = 8.00$ %, $R_p = 5.77$ %, and $\chi^2 = 1.137$, indicating the reliability of the refined results and the single-phase nature of the phosphor.

The crystal structure of NGP was characterized by $(PO_3)_n$-helix bands composed of PO_4 tetrahedra sharing common vertex angles. These bands extend infinitely around the c-axis, with a periodic repeating unit of n = 4. Each tetrahedron shares two oxygen atoms with neighboring tetrahedra. Gd^{3+} ions are located between two helical bands, forming distorted GdO_8 dodecahedra that are isolated from each other. Na^+ ions occupy irregular voids forming NaO_6 polyhedra which extend into serrated junctions.

The SEM images of NGP:20Yb0.5Er in Fig. 1c reveal the bulk nature of crystals on micro size. The elemental analysis in Fig. 1d demonstrates the uniform distribution of the Yb^{3+} and Er^{3+} dopants. Furthermore, EDS analysis (Fig. 1e) confirms the presence of the expected elements in the prepared NGP:20Yb0.5Er sample.

3.2. Raman, UV–Vis and DFT

Raman spectroscopy was performed for the NGP host matrix, as shown in Fig. 2a. Both cases exhibit two intense peaks at 699 cm^{-1} and 1184 cm^{-1}, which belong to the symmetric stretching vibration modes of P-O-P and O-P-O bonds respectively. These peaks are characteristic of long-chain polyphosphates with a maximum phonon energy of 1300 cm^{-1}.

Fig. 2b depicts the UV–Vis diffuse reflectance spectrum of the NGP:20Yb0.5Er sample exhibiting characteristic f-f transitions of Er^{3+}. Notably, the reflectivity exceeds 100 % in the range of 200–300 nm due to the induced emitting photons excited by these UV photons. The emission light consists of not only Er^{3+} emitting photons in the visible range but also Gd^{3+} emitting photons in the red region ($^6G_J \rightarrow {}^6P_J$) [17]. The peak around 270 nm corresponds to the $^8S_{7/2} \rightarrow {}^6D_J$ transition of Gd^{3+} ions in the host NGP.

To gain insights into the electronic structure of NGP, DFT calculations were performed based on the first principles. The maximum valence band is primarily contributed by the 4f orbitals of Gd^{3+}, while the minimum conduction band is mainly attributed to the outermost orbitals of O^{2-} and Na^+ (Fig. 2c). The calculated band gap is 4.18 eV (Fig. 2d).

3.3. Upconversion luminescence

The dopant concentration was optimized by quantifying the integral emission intensity. The optical Yb^{3+} concentration was

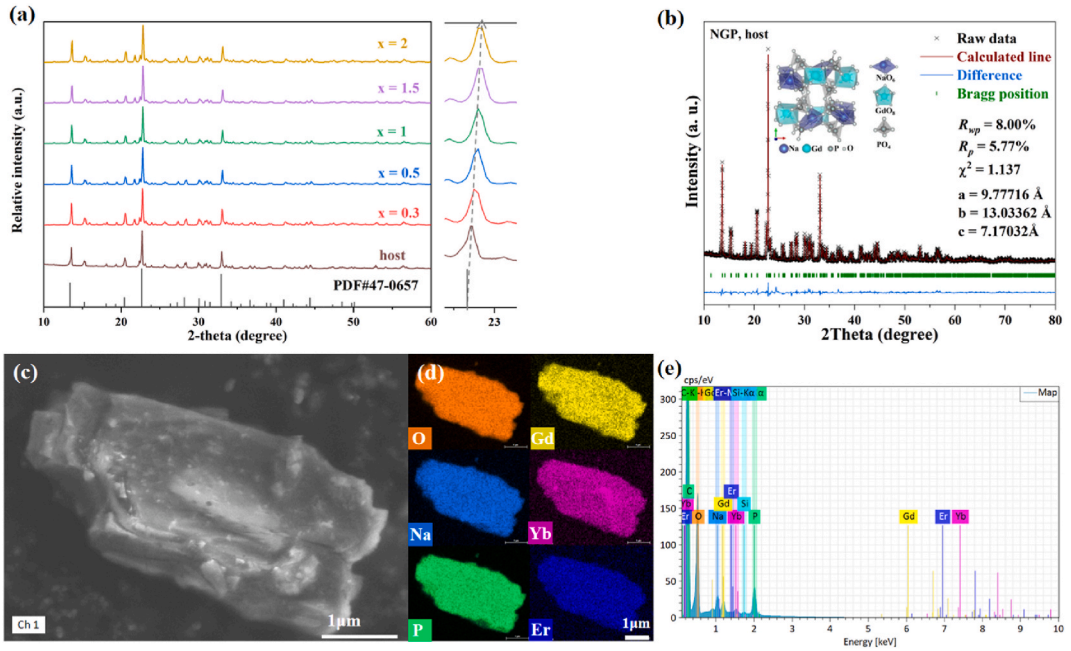

Fig. 1. (a) XRD patterns of NGP:20YbxEr (x = 0.3, 0.5, 1, 1.5, 2 at%) samples and NGP host referring to the standard pattern of NGP; (b) Rietveld refinement of the XRD pattern for the host matrix showing the crystal structure; (c) A SEM image of NGP:20Yb0.5Er with corresponding (d) elemental mapping and (e) EDS spectra.

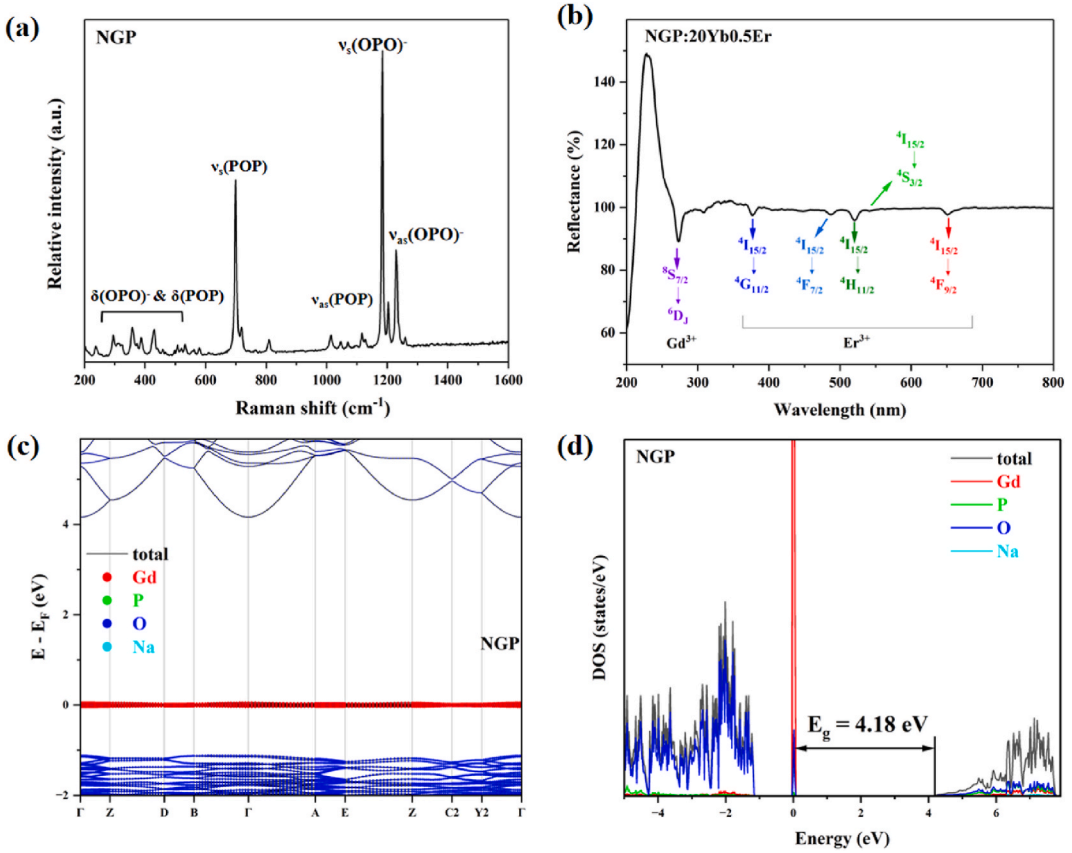

Fig. 2. (a) Raman spectra of the NGP host; (b) UV–Vis diffuse reflectance spectrum of NGP:20Yb0.5Er; (c) Electronic band structure of NGP; (d) Density of states of NGP.

determined to be 20 at% achieving the most intense UC luminescence (Fig. S2). Excessive Yb^{3+} concentration would cause significant Yb^{3+}-Yb^{3+} energy transfer and Er^{3+} to Yb^{3+} energy-back-transfer (EBT) [23]. The optimal Er^{3+} concentration was found to be 0.5 at% (Fig. 3a) as a higher dopant concentration would lead to common concentration quenching [24]. The reason that Na^+ ions incorporated phosphors were selected is that $NaGd(PO_3)_4$:20Yb0.5Er exhibited superior UC emission intensity under 980 nm laser excitation compared to K^+ (3-fold) and Li^+ (13-fold) hosted counterparts (Fig. S3). This may be due to the low site symmetry of lanthanide ions induced by the Na^+ incorporation [25] (Table S1).

The emission spectra of NGP:20YbxEr (x = 0.3, 0.5, 1, 1.5, 2 at%) show characteristic Er^{3+} green emission at 524 nm and 550 nm (due to $^2H_{11/2}$/$^4S_{3/2} \rightarrow {}^4I_{15/2}$ transition) and red emission at 657 nm (due to $^4F_{9/2} \rightarrow {}^4I_{15/2}$ transition) in Fig. 3a, and it can be found that 0.5 at% Er^{3+} is the optimal concentration. The red and green emission intensity ratios (I_R/I_G) of the NGP:20YbxEr samples continually decrease with the increase of Er^{3+} ion concentration, indicating that the red emission of Er^{3+} ions in the NGP host is more affected by the concentration quenching compared to green emission. The same tendency is present in both Yb/Er co-doped $LiGd(PO_3)_4$ and $KGd(PO_3)_4$ phosphors (Fig. S4), which is consistent with the report about $ZnGa_2O_4$:Er^{3+}/Yb^{3+} [26].

The relationship between UC emission intensity (I) and pump laser power (P) is nonlinear, expressed as:

$$I \propto P^n \tag{2}$$

where n represents the number of excitation photons required to reach the emitting excited state. The respective emission intensity integrated from the power-dependent emission spectra of NGP:20Yb0.5Er is plotted with the excitation power, yielding n values of 1.8 for green emission and 1.6 for red emission (Fig. 3b). It demonstrates that both the red and green UC emissions primarily involve a two-photon process. As illustrated in Fig. 3c, under 980 nm laser excitation, Yb^{3+} ions absorb the photon energy and transfer it to the neighboring Er^{3+} ions. Er^{3+} ions in the ground state $^4I_{15/2}$ are excited through ground state absorption and excited state absorption to $^2H_{11/2}$, $^4S_{3/2}$, and $^4F_{9/2}$ levels with non-radiative relaxation (NR). Upon increasing the Er^{3+} concentration, multiple cross-relaxation (CR) processes between Er^{3+} ions [CR_1: $^4S_{3/2}+{}^4I_{15/2} \rightarrow {}^4I_{9/2}+{}^4I_{13/2}$, CR_2: $^4F_{7/2}+{}^4I_{11/2} \rightarrow {}^4F_{9/2}+{}^4F_{9/2}$, CR_3: $^2H_{11/2}+{}^4I_{13/2} \rightarrow {}^4F_{9/2}+{}^4I_{11/2}$] and the energy-back-transfer from Er^{3+} to Yb^{3+} [$^4S_{3/2}$ (Er)+$^2F_{7/2}$ (Yb)→$^4I_{13/2}$ (Er)+$^2F_{5/2}$ (Yb)] can occur [27,28].

Subsequently, to gain more insight into the photon processes, photoluminescence time-resolved spectra were measured. The decays at 550 and 524 nm keep the same as they are thermally coupled with a very small gap. Therefore the decay lifetimes were just calculated for the green (550 nm, $^2H_{11/2} \rightarrow {}^4I_{15/2}$) and red emissions (657 nm, $^4F_{9/2} \rightarrow {}^4I_{15/2}$). The energy transfer process of Yb-Er is

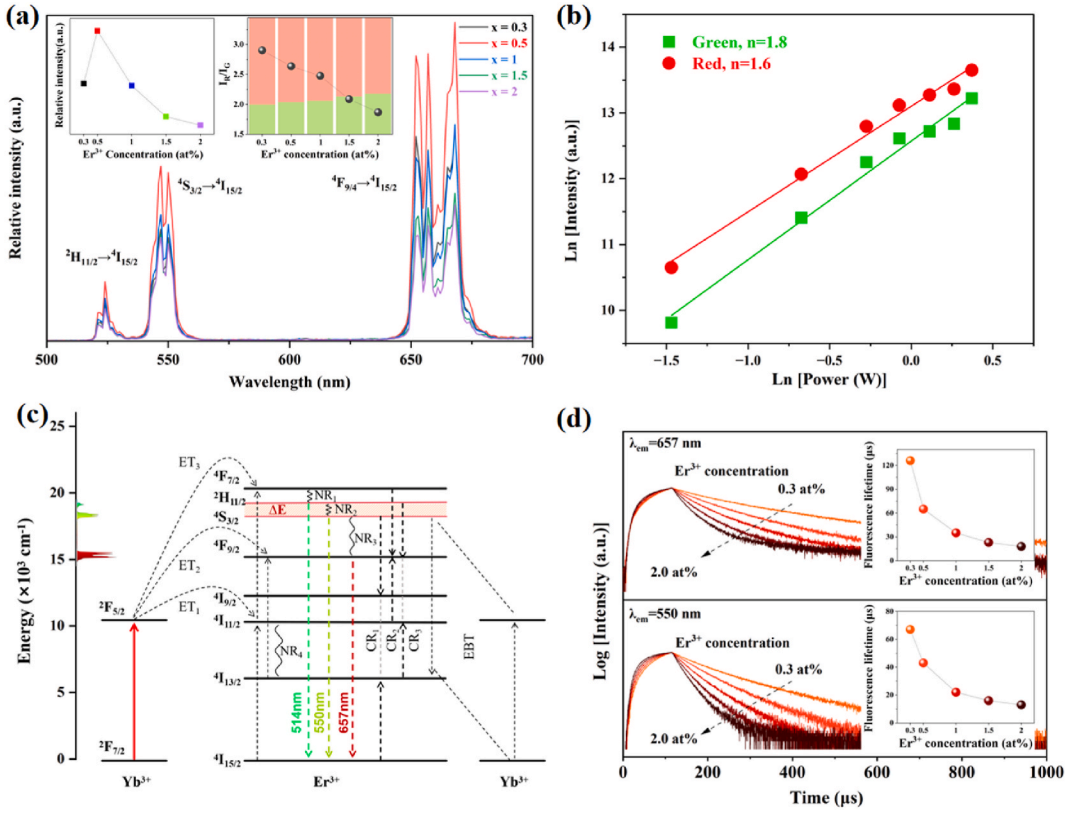

Fig. 3. (a) UC emission spectra of NGP:20YbxEr (x = 0.3, 0.5, 1, 1.5, 2 at%) with insets of Er^{3+} concentration-dependent emission intensity and I_R/I_G ratio; (b) Pump power dependence of the UC emission intensity in NPG:20Yb0.5Er; (c) Energy level diagram for the Yb^{3+}-Er^{3+} couple, indicating the energy transfer, cross-relaxation, and UC emissions; (d) Luminescence decay curves of red and green emissions in NGP:20YbxEr (x = 0.3, 0.5, 1, 1.5, 2 at%) and the inset plots of lifetime vs. Er^{3+} concentration. (For interpretation of the references to colour in this figure legend, the reader is referred to the Web version of this article.)

obvious so that the curve of attenuation kinetics can be fitted using the double exponential function Eq. (3):

$$I(t) = A_1 \exp(-t/\tau_1) + A_2 \exp(-t/\tau_2) \quad (3)$$

where I and t are the luminescence intensity and time, A_1 and A_2 are the fitting parameters, and τ_1 and τ_2 are the long and short lifetimes, respectively. The average fluorescence lifetime τ is calculated by Eq. (4):

$$T_{av} = \left(A_1\tau_1^2 + A_2\tau_2^2\right) / \left(A_1\tau_1 + A_2\tau_2\right) \quad (4)$$

As a result, the lifetime of the three characteristic peaks of NGP:Yb^{3+}/Er^{3+} is basically manifested as $\tau_{550\ nm} < \tau_{657\ nm}$, which is consistent with the intensity of the two peaks (Fig. 3d). As the Er^{3+} concentration increases, the decay lifetimes of the green and red emissions gradually decrease due to the concentration quenching. Notably, the red emission lifetime is dramatically shortened by 50 % with a slight Er^{3+} concentration increase from 0.3 at% to 0.5 at% (vs. a 35 % drop for the green emission lifetime). This result is consistent with the decrease of I_R/I_G and the same tendency in Er^{3+} concentration-dependent lifetime, which can also be found in the host KGP and LGP (Fig. S5). The significant lifetime reduction of the red emitting level is attributed to the CR and EBT processes. Meanwhile, the rise time is shortened evidently with the increase of Er^{3+} concentration (Fig. S6), which indicates the UC transition probability is elevated owing to the enhanced interaction between Yb^{3+} and Er^{3+} ions.

3.4. Optical thermal sensing

In order to study the optical thermal properties of the obtained polyphosphate phosphor, the temperature-dependent UC emission spectra of the NGP:20Yb0.5Er phosphor were measured. The UC emission intensity of the sample NGP:20Yb0.5Er (Fig. 4a) gradually decreases with temperature increasing in the range of 77–573 K, which is in agreement with the phenomenon caused by the conventional thermal quenching [29]. This is because the increase in temperature consumes the excitation energy of the luminescent center in the form of more lattice vibrations, resulting in a decrease in luminous efficiency [30]. Lower temperatures can reduce thermodynamic lattice vibrations, resulting in the appearance of sharp lines with fine structures. At 77 K, the $^4F_{9/2} \rightarrow {}^4I_{15/2}$ transition

emission of Er^{3+} is split into more peaks due to the effect of the crystal field (Fig. 4b). The $^2H_{11/2} \rightarrow {}^4I_{15/2}$ transition is absent at low temperature and only appears when the temperature reaches 200 K. Upon further increasing the temperature, its emission intensity initially increases until 425 K due to the thermal activation to the upper thermally coupled state [31]. It can be found that the I_R/I_G ratio decreases as temperature rises, suggesting that the red emitting level is more sensitive to temperature quenching. The temperature-dependent decay curves in Fig. 4c show an almost unchanged lifetime, suggesting that the thermal quenching effect is limited for luminescence dynamics of the green and red emission in the NPG host. This phenomenon was also observed in $Na_3Sc_2(PO_4)_3$:Yb/Er phosphors [32].

Based on the previous results, the thermal sensing ability of the NGP:Yb/Er phosphors in the temperature range from 200 K to 573 K can be explored. The technique of fluorescence intensity ratio (FIR) is used for the thermally coupled energy levels $^2H_{11/2}$ and $^4S_{3/2}$, expressed as [33]:

$$FIR_{524/550} = \frac{I_{524}}{I_{550}} = B\,exp(-\Delta E / k_B T) \tag{5}$$

where I, B, ΔE, k_B and T represent the integrated emission intensity, a constant, energy difference between thermally coupled states, Boltzmann constant and absolute temperature, respectively. Fig. 4d plots the FIR as a function of temperature. The fitted result suggests the thermal sensing ability maintained in a wide range of 200–573 K. The energy difference ΔE between the $^2H_{11/2}$ and $^4S_{3/2}$ levels is determined to be 721.73 cm^{-1}, which is very close to the energy difference of about 700 cm^{-1} in literature [5].

The practical application of thermal probes using UC phosphors relies on two key parameters, absolute thermal sensitivity (S_a) and relative thermal sensitivity (S_r), determined as follows [7]:

$$S_a = \left|\frac{\partial FIR}{\partial T}\right| = FIR\frac{\Delta E}{KT^2} \tag{6}$$

$$S_r = \left|\frac{1}{FIR}\frac{\partial FIR}{\partial T}\right| = \frac{\Delta E}{KT^2} \tag{7}$$

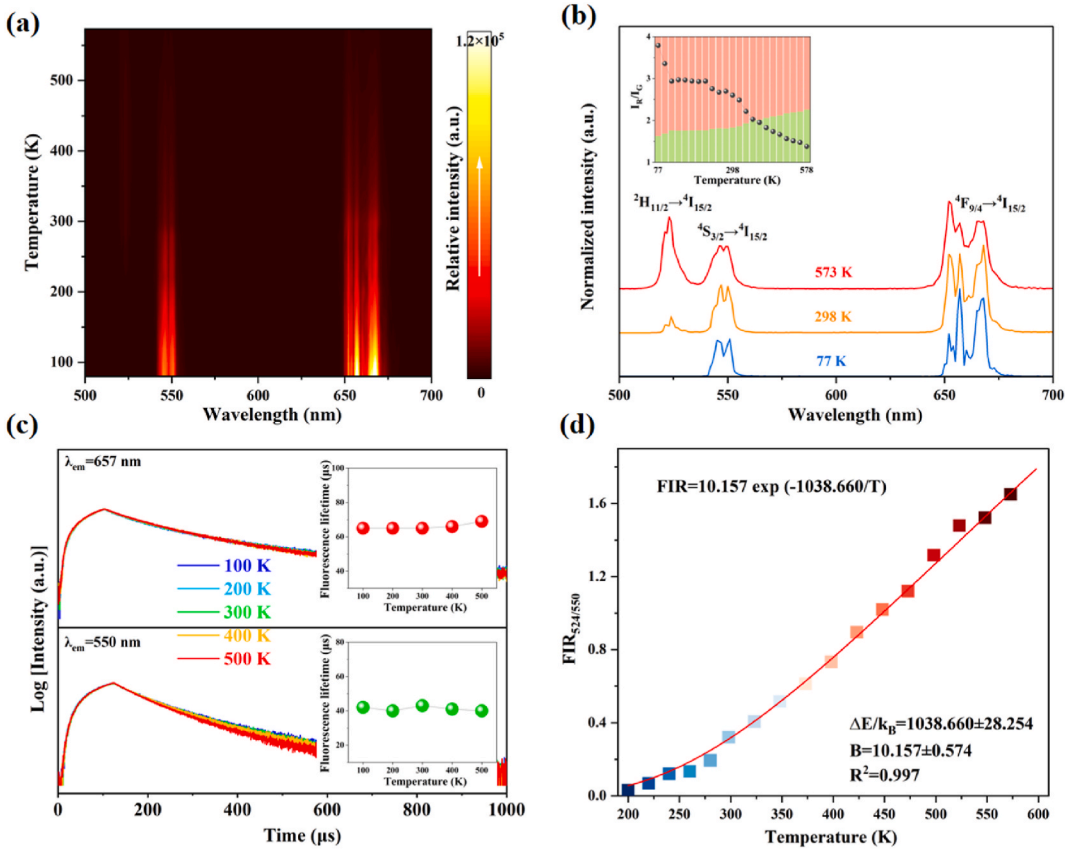

Fig. 4. (a) Temperature-dependent UC emission intensity map of the NPG:20Yb0.5Er phosphor. (b) UC emission spectra at the temperature of 77, 298, 573 K showing the tendency of I_R/I_G as temperature increases. (c) Temperature-dependent decay curves of the red and green emitting levels with the lifetime quantification as insets. (d) Temperature-dependent $FIR_{524/550}$. (For interpretation of the references to colour in this figure legend, the reader is referred to the Web version of this article.)

In the range of 200–573 K, both parameters S_a and S_r of NGP:20Yb0.5Er as a function of temperature were plotted and fitted in Fig. 5a. As the temperature increases, the absolute thermal sensitivity S_a increases and reaches the maximum of 0.53 % K^{-1} at 523 K. The relative thermal sensitivity S_r decreases monotonically with a maximum value of 2.60 % K^{-1} at 200 K. This performance in NGP:20Yb0.5Er is compared with those of other oxide materials based on Er^{3+} thermally coupled energy levels in Table 1. The NGP:20Yb0.5Er in this work exhibits moderate thermal sensitivity and is superior to $Na_3Gd(VO_4)_2$, $NaZr_2(PO_4)_3$ and β-$NaYF_4$, which indicates its potential applications in non-contact optical thermal sensing.

Furthermore, thermal repeatability which is another crucial factor for practical applications was also assessed (Fig. 5b) using the following equation [40]:

$$R = 1 - \frac{Max|FIR_a - FIR_i|}{FIR_a} \tag{8}$$

where FIR_a is the average FIR value and FIR_i is the measured FIR value during the temperature cycling process. The thermal repeatability in this work was found to be greater than 97 %, which further indicates the high precision of the thermal sensing ability of NGP:Yb/Er phosphors.

4. Conclusions

NGP:20YbxEr (x = 0.3, 0.5, 1, 1.5, 2 at%) phosphors were successfully synthesized using a high-temperature solid-phase method. The optimal Er^{3+} doping concentration was determined to be 0.5 at%. Under 980 nm laser excitation, the phosphors exhibited green emission ($^2H_{11/2}$, $^4S_{3/2} \rightarrow {}^4I_{15/2}$) and red emission ($^4F_{9/4} \rightarrow {}^4I_{15/2}$) through two-photon energy transfer processes. Notably, the NGP host demonstrated superior luminescence efficiency compared to KGP and LGP, primarily attributed to its asymmetric lattice structure and site. Due to the effect of complex multiple cross-relaxation, the I_R/I_G ratio decreased with the increasing Er^{3+} ion concentration attributed to complex cross-relaxation processes. Additionally, the obtained phosphors show a gradual decrease in the decay lifetime of both green and red emissions due to concentration quenching. The obtained NGP:20Yb0.5Er phosphor exhibits good temperature sensing capabilities, achieving a maximum absolute sensitivity S_a of 0.53 % K^{-1} at 523 K and a maximum relative sensitivity S_r of 2.6 % K^{-1}. The fluorescence intensity ratio FIR demonstrated remarkable reproducibility over heating-cooling cycles, confirming the phosphor's thermal stability. These findings highlight the significant potential of NGP:20Yb0.5Er as a promising material for optical thermal sensing applications.

CRediT authorship contribution statement

Jintao Xu: Writing – review & editing, Writing – original draft, Formal analysis, Data curation. **Shanlin Zhu:** Writing – review & editing. **Canyuan Liao:** Validation, Software. **Weijun Zhao:** Writing – review & editing. **Xingyuan Zhong:** Writing – review & editing. **Zijun Wang:** Writing – review & editing, Funding acquisition. **Jiuping Zhong:** Writing – review & editing, Supervision, Funding acquisition.

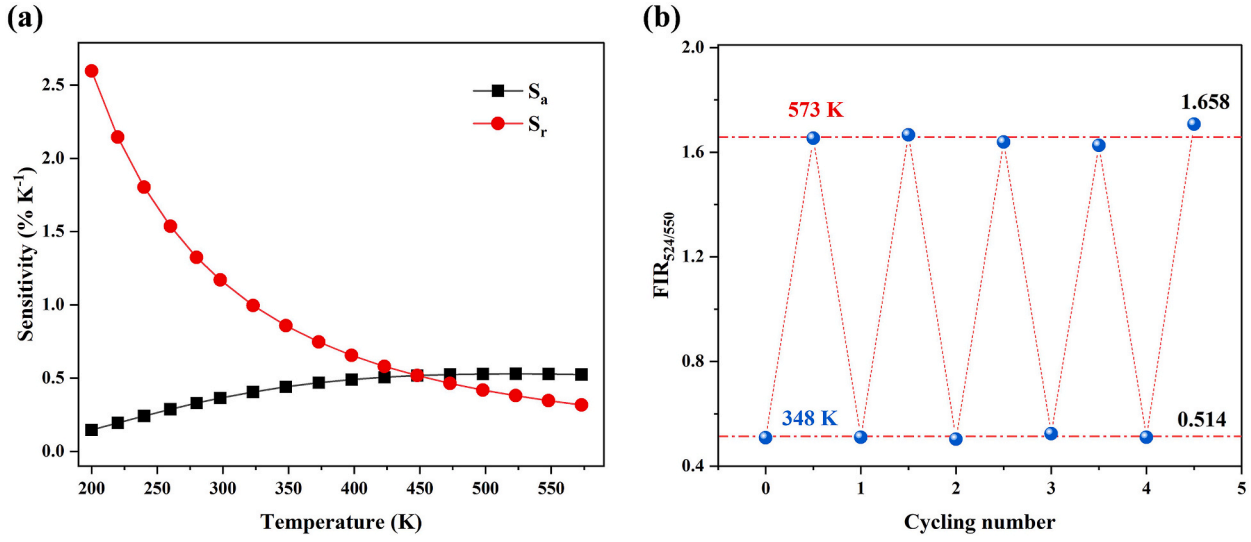

Fig. 5. (a) Temperature-dependent thermal sensitivity of S_a and S_r for NGP:20Yb0.5Er. (b) $FIR_{524/550}$ under thermal cycling (348–573 K).

Table 1
A list of thermal sensing characteristics of Er^{3+}/Yb^{3+} co-doped UC phosphors using thermally coupled energy levels of Er^{3+}.

Host	Temperature range (K)	$S_{a\ max}$ (K^{-1})	Ref.
$SrWO_4$	300–518	1.50 % (403K)	[10]
$CaMoO_4$	303–873	1.43 % (573K)	[11]
$YNbO_4$	300–573	0.73 % (473K)	[12]
$LiLuW_2O_8$	300–500	0.57 % (500K)	[34]
$NaGd(PO_3)_4$	200–598	0.53 % (548K)	This work
Al_2O_3	295–973	0.51 % (495K)	[35]
$Na_3Gd(VO_4)_2$	291–578	0.48 % (578K)	[36]
$NaZr_2(PO_4)_3$	303–573	0.41 %(461K)	[37]
Gd_2O_3	300–900	0.39 % (300K)	[38]
β-$NaYF_4$	223–403	0.37 % (363K)	[39]

Additional information

See Supplementary Information for supporting content.

Data availability statement

Data will be made available on request.

Declaration of competing interest

The authors declare the following financial interests/personal relationships which may be considered as potential competing interests: Jiuping Zhong reports financial support was provided by National Natural Science Foundation of China (62275276, 21771196). Jiuping Zhong reports a relationship with National Natural Science Foundation of China (62275276, 21771196) that includes: funding grants. If there are other authors, they declare that they have no known competing financial interests or personal relationships that could have appeared to influence the work reported in this paper.

Acknowledgments

This work was funded by National Natural Science Foundation of China (62275276, 21771196). The authors thank Yanan Fan (School of Chemistry, Sun Yat-sen University) for assistance in the measurements of UV–Vis diffuse reflectance spectroscopy and fluorescence spectroscopy, Shengcai Zhu (School of Materials, Sun Yat-sen University) for providing DFT computing resources, and Yingliang Zhao (School of Materials, Sun Yat-sen University) for conducting DFT calculation.

Appendix A. Supplementary data

Supplementary data to this article can be found online at https://doi.org/10.1016/j.heliyon.2024.e39951.

References

[1] B. Dong, B. Cao, Y. He, et al., Temperature sensing and in vivo imaging by molybdenum sensitized visible upconversion luminescence of rare-earth oxides, Adv. Mater. 24 (15) (2012) 1987–1993, https://doi.org/10.1002/adma.201200431.
[2] B. Zhou, L. Yan, J. Huang, et al., NIR II-responsive photon upconversion through energy migration in a ytterbium sublattice, Nat. Photonics 14 (12) (2020) 760–766, https://doi.org/10.1038/s41566-020-00714-6.
[3] A.A. Ansari, A.K. Parchur, Y. Li, et al., Cytotoxicity and genotoxicity evaluation of chemically synthesized and functionalized upconversion nanoparticles, Coord. Chem. Rev. 504 (2024) 215672, https://doi.org/10.1016/j.ccr.2024.215672.
[4] Y. Liu, Y. Lu, X. Yang, et al., Amplified stimulated emission in upconversion nanoparticles for super-resolution nanoscopy, Nature 543 (7644) (2017) 229–233, https://doi.org/10.1038/nature21366.
[5] X. Wang, Q. Liu, Y. Bu, et al., Optical temperature sensing of rare-earth ion doped phosphors, RSC Adv. 5 (105) (2015) 86219–86236, https://doi.org/10.1039/C5RA16986K.
[6] S.A. Wade, S.F. Collins, G.W. Baxter, Fluorescence intensity ratio technique for optical fiber point temperature sensing, J. Appl. Phys. 94 (8) (2003) 4743–4756, https://doi.org/10.1063/1.1606526.
[7] Q. Wang, M. Liao, Q. Lin, et al., A review on fluorescence intensity ratio thermometer based on rare-earth and transition metal ions doped inorganic luminescent materials, J. Alloy. Compd. 850 (2021) 156744, https://doi.org/10.1016/j.jallcom.2020.156744.
[8] A. Shandilya, R.S. Yadav, A.K. Gupta, et al., Effects of Yb^{3+} ion doping on lattice distortion, optical absorption and light upconversion in Er^{3+}/Yb^{3+} co-doped $SrMoO_4$ ceramics, Mater. Chem. Phys. 264 (2021) 124441, https://doi.org/10.1016/j.matchemphys.2021.124441.
[9] T. Li, C. Guo, L. Li, Up-conversion luminescence of Er^{3+}-Yb^{3+} Co-doped $CaIn_2O_4$, Opt Express 21 (15) (2013) 18281–18289, https://doi.org/10.1364/OE.21.018281.
[10] A. Pandey, V.K. Rai, V. Kumar, et al., Upconversion based temperature sensing ability of Er^{3+}–Yb^{3+}codoped $SrWO_4$: an optical heating phosphor, Sens. Actuator B-Chem. 209 (2015) 352–358, https://doi.org/10.1016/j.snb.2014.11.126.

[11] F. Huang, Y. Gao, J. Zhou, et al., Yb^{3+}/Er^{3+} Co-doped $CaMoO_4$: a promising green upconversion phosphor for optical temperature sensing, J. Alloy. Compd. 639 (2015) 325–329, https://doi.org/10.1016/j.jallcom.2015.02.228.

[12] A.K. Singh, S.K. Singh, B.K. Gupta, et al., Probing a highly efficient dual mode: down–upconversion luminescence and temperature sensing performance of rare-earth oxide phosphors, Dalton Trans. 42 (4) (2012) 1065–1072, https://doi.org/10.1039/C2DT32054A.

[13] R. S. Yadav Monika, A. Bahadur, et al., Concentration and pump power-mediated color tunability, optical heating and temperature sensing via TCLs of red emission in an $Er^{3+}/Yb^{3+}/Li^{+}$ Co-doped $ZnGa_2O_4$ phosphor, RSC Adv. 9 (68) (2019) 40092–40108, https://doi.org/10.1039/C9RA09120C.

[14] R.S. Yadav, D. Kumar, A.K. Singh, et al., Effect of Bi^{3+} ion on upconversion-based induced optical heating and temperature sensing characteristics in the Er^{3+}/Yb^{3+} Co-doped La_2O_3 nano-phosphor, RSC Adv. 8 (60) (2018) 34699–34711, https://doi.org/10.1039/C8RA07438K.

[15] L. Zheng, X. Huang, J. Zhong, et al., Upconversion luminescence and temperature sensing properties of $NaGd(WO_4)_2$:Yb^{3+}/Er^{3+}@SiO_2 core-shell nanoparticles, RSC Adv. 11 (7) (2021) 3981–3989, https://doi.org/10.1039/D0RA10039K.

[16] A. Shandilya, R.S. Yadav, A.K. Gupta, et al., Temperature-dependent light upconversion and thermometric properties of Er^{3+}/Yb^{3+}-codoped $SrMoO_4$ sintered ceramics, J. Mater. Sci. 56 (22) (2021) 12716–12731, https://doi.org/10.1007/s10853-021-06078-8.

[17] J. Zhong, H. Liang, Q. Su, et al., Luminescence properties of $NaGd(PO_3)_4$:Eu^{3+} and energy transfer from Gd^{3+} to Eu^{3+}, Appl. Phys. B 98 (1) (2010) 139–147. https://link.springer.com/article/10.1007/s00340-009-3673-y.

[18] P. Hohenberg, W. Kohn, Inhomogeneous electron gas, Phys. Rev. 136 (3B) (1964) B864–B871, https://doi.org/10.1103/PhysRev.136.B864.

[19] J.P. Perdew, K. Burke, M. Ernzerhof, Generalized gradient approximation made simple, Phys. Rev. Lett. 77 (18) (1996) 3865–3868, https://doi.org/10.1103/PhysRevLett.77.3865.

[20] S.L. Dudarev, G.A. Botton, S.Y. Savrasov, et al., Electron-energy-loss spectra and the structural stability of nickel oxide: an LSDA+U study, Phys. Rev. B 57 (3) (1998) 1505–1509, https://doi.org/10.1103/PhysRevB.57.1505.

[21] D. van der Marel, G.A. Sawatzky, Electron-electron interaction and localization in d and f transition metals, Phys. Rev. B 37 (18) (1988) 10674–10684, https://doi.org/10.1103/PhysRevB.37.10674.

[22] I. Parreu, M.C. Pujol, M. Aguiló, et al., Growth, spectroscopy and laser operation of Yb:$KGd(PO_3)_4$ single crystals, Opt Express 15 (5) (2007) 2360–2368, https://doi.org/10.1364/OE.15.002360.

[23] X. Li, J. Li, X. Xu, et al., Bi^{3+} assisted enhancement of photoluminescence and thermal sensing of Er^{3+}/Yb^{3+} Co-doped $SrGdAlO_4$ phosphor with unusual stable color, Ceram. Int. 47 (6) (2021) 8538–8544, https://doi.org/10.1016/j.ceramint.2020.11.221.

[24] D.C. Yeh, W.A. Sibley, M. Suscavage, et al., Multiphonon relaxation and infrared-to-visible conversion of Er^{3+} and Yb^{3+} ions in barium-thorium fluoride glass, J. Appl. Phys. 62 (1) (1987) 266–275, https://doi.org/10.1063/1.339139.

[25] L. Wang, X. Li, Z. Li, et al., A new cubic phase for a $NaYF_4$ host matrix offering high upconversion luminescence efficiency, Adv. Mater. 27 (37) (2015) 5528–5533, https://doi.org/10.1002/adma.201502748.

[26] R. S. Yadav Monika, A. Bahadur, et al., Concentration and pump power-mediated color tunability, optical heating and temperature sensing via TCLs of red emission in an $Er^{3+}/Yb^{3+}/Li^{+}$ Co-doped $ZnGa_2O_4$ phosphor, RSC Adv. 9 (68) (2019) 40092–40108, https://doi.org/10.1039/C9RA09120C.

[27] F. Liu, E. Ma, D. Chen, et al., Tunable red-green upconversion luminescence in novel transparent glass ceramics containing Er:$NaYF_4$ nanocrystals, J. Phys. Chem. B 110 (42) (2006) 20843–20846, https://doi.org/10.1021/jp063145m.

[28] D. Xu, C. Liu, J. Yan, et al., Understanding energy transfer mechanisms for tunable emission of Yb^{3+}-Er^{3+} codoped GdF_3 nanoparticles: concentration-dependent luminescence by near-infrared and violet excitation, J. Phys. Chem. C 119 (12) (2015) 6852–6860, https://doi.org/10.1021/acs.jpcc.5b00882.

[29] R. S. Yadav Monika, A. Rai, et al., NIR light guided enhanced photoluminescence and temperature sensing in $Ho^{3+}/Yb^{3+}/Bi^{3+}$ Co-doped $ZnGa_2O_4$ phosphor, Sci. Rep. 11 (1) (2021) 4148, https://doi.org/10.1038/s41598-021-83644-9.

[30] J. Liao, M. Wang, F. Lin, et al., Thermally boosted upconversion and downshifting luminescence in $Sc_2(MoO_4)_3$:Yb/Er with two-dimensional negative thermal expansion, Nat. Commun. 13 (1) (2022) 2090, https://doi.org/10.1038/s41467-022-29784-6.

[31] Z. Wang, J. Christiansen, D. Wezendonk, et al., Thermal enhancement and quenching of upconversion emission in nanocrystals, Nanoscale 11 (25) (2019) 12188–12197, https://doi.org/10.1039/C9NR02271F.

[32] S. Wang, Y. Wang, Z. Tao, et al., Distinct thermal quenching of upconversion and downshifting luminescence caused by dynamic defects in ion-conductive $Na_3Sc_2(PO_4)_3$:Yb^{3+}, Er^{3+} phosphor, Chin. J. Lumin. 45 (6) (2024) 863–875, https://doi.org/10.37188/CJL.20240073.

[33] D. Jaque, F. Vetrone, Luminescence nanothermometry, Nanoscale 4 (15) (2012) 4301–4326, https://doi.org/10.1039/C2NR30764B.

[34] X. Yun, J. Zhou, Y. Zhu, et al., Green up-conversion luminescence and optical thermometry of Yb^{3+}/Er^{3+} Co-doped $LiLuW_2O_8$ phosphor, J. Phys. Chem. Solids 163 (2022) 110545, https://doi.org/10.1016/j.jpcs.2021.110545.

[35] B. Dong, D.P. Liu, X.J. Wang, et al., Optical thermometry through infrared excited green upconversion emissions in Er^{3+}–Yb^{3+} codoped Al_2O_3, Appl. Phys. Lett. 90 (18) (2007) 181117, https://doi.org/10.1063/1.2735955.

[36] K. Saidi, M. Dammak, K. Soler-Carracedo, et al., Optical thermometry based on upconversion emissions in $Na_3Gd(VO_4)_2$: Yb^{3+}-Er^{3+}/Ho^{3+} micro crystals, J. Alloy. Compd. 891 (2022) 161993, https://doi.org/10.1016/j.jallcom.2021.161993.

[37] L. Mukhopadhyay, S. Pattnaik, V.K. Rai, Spectroscopic in-depths of upconverting $NaZr_2(PO_4)_3$ phosphors for LIR-based thermometry, RSC Adv. 13 (30) (2023) 21096–21104, https://doi.org/10.1039/D3RA02126B.

[38] S.K. Singh, K. Kumar, S.B. Rai, Er^{3+}/Yb^{3+} codoped Gd_2O_3 nano-phosphor for optical thermometry, Sens. Actuator A-Phys. 149 (1) (2009) 16–20, https://doi.org/10.1016/j.sna.2008.09.019.

[39] B. Dong, R.N. Hua, B.S. Cao, et al., Size dependence of the upconverted luminescence of $NaYF_4$:Er, Yb microspheres for use in ratiometric thermometry, Phys. Chem. Chem. Phys. 16 (37) (2014) 20009–20012, https://doi.org/10.1039/C4CP01966K.

[40] A. Nexha, J.J. Carvajal, M.C. Pujol, et al., Lanthanide doped luminescence nanothermometers in the biological windows: strategies and applications, Nanoscale 13 (17) (2021) 7913–7987, https://doi.org/10.1016/bs.hpcre.2016.03.005.